RSC Advances

PAPER

View Article Online
View Journal | View Issue

Cite this: *RSC Adv.*, 2014, **4**, 18842

Assessing the critical concentration of NH_2 terminal groups on the surface of MWNTs towards chain scission of PC in PC/SAN blends: effect on dispersion, electrical conductivity and EMI shielding

Shital Patangrao Pawar, K. Pattabhi and Suryasarathi Bose*

Received 24th February 2014
Accepted 7th April 2014

DOI: 10.1039/c4ra01610f

www.rsc.org/advances

The localization and dispersion quality of as received NH_2 terminated multiwall carbon nanotubes (MWNT-I) and ethylene diamine (EDA) functionalized MWNTs in melt mixed blends of polycarbonate (PC) and poly(styrene-*co*-acrylonitrile) (SAN) were assessed in this study using rheo-electrical and electromagnetic interference (EMI) shielding measurements. In order to improve the dispersion quality and also to selectively localize MWNTs in the PC phase of the blends, EDA was grafted onto MWNTs by two different strategies like diazonium reaction of the *para*-substituted benzene ring of MWNTs with EDA (referred to as MWNT-II) and acylation of carboxyl functionalized MWNTs with thionyl chloride (referred to as MWNT-III). By this approach we could systematically vary the concentration of NH_2 functional groups on the surface of MWNTs at a fixed concentration (1 wt%) in PC/SAN blends. XPS was carried to evaluate the % concentration of N in different MWNTs and was observed to be highest for MWNT-III manifesting in a large surface coverage of EDA on the surface of MWNTs. Viscoelastic properties and melt electrical conductivities were measured to assess the dispersion quality of MWNTs using a rheo-electrical set-up both in the quiescent as well as under steady shear conditions. Rheological properties revealed chain scission of PC in the presence of MWNT-III which is due to specific interactions between EDA and PC leading to smaller PC grafts on the surface of MWNTs. The observed viscoelastic properties in the blends were further correlated with the phase morphologies under quiescent and annealed conditions. Electromagnetic interference (EMI) shielding effectiveness in X and K_u-band frequencies were measured to explore these composites for EMI shielding applications. Interestingly, MWNT-II showed the highest electrical conductivity and EMI shielding in the blends.

Introduction

In order to design tailor-made properties in macromolecules, often they are blended either with another macromolecule or with nanoparticles. The latter strategy is adopted to accomplish the extensive use of nanocomposites for wide range of applications. Specific interactions between the blend components govern the thermodynamic miscibility in polymer blends. However, due to high molecular weight and a very small gain in entropy of mixing, most often the pairs are immiscible in nature. The latter phenomenon results in various types of morphology during processing which can then be utilized for different applications.

Since, polymers are electrically insulating in nature, addition of conducting fillers like carbon nanotubes (CNTs) can render high electric conductivity in the composites.[1–7] However, in order to realize the exceptional properties associated with CNTs, uniform dispersion is very crucial. Alternatively, higher electrical conductivity can be achieved by adopting the concept of double percolation.[8] This is accomplished by selectively localizing conducting particles in a given phase of a co-continuous blend. This strategy can often yield high electrical conductivity at relatively lower fraction of conducting particles.

CNTs, owing to their high aspect ratio, facilitates percolating network at relatively lower concentration and hence, a great deal of research focuses on the electrical conductivity of polymer/CNT composites.[9,10] It is understood, that aggregated CNTs in turn reduces the effective aspect ratio in striking contrast to well dispersed CNTs. Various strategies have been adopted to address the issues related to uniform dispersion of CNTs in polymer matrix. Electric conductivity of CNTs is dependent on π-conjugation.[11] In non-covalent approach, π-electron cloud on CNT surface enable the adsorption of various moieties and the integrity of CNTs is preserved whereas, covalent modification of

Department of Materials Engineering, Indian Institute of Science, Bangalore-560012, India. E-mail: sbose@materials.iisc.ernet.in

CNTs affects the band gap at Fermi level and deteriorates the electrical properties.[12]

Electromagnetic radiations emitted by commercial appliances, military and scientific equipment and communication devices are continuously increasing. In order to protect the workspace and environment from external electromagnetic radiations, materials that can shield the external electromagnetic interference are in great demand. Polymer based conducting nanocomposites as EMI shielding materials offer unique advantage over conventional materials due to its flexibility and ease of processing, high strength to weight ratio, corrosion resistance and tunable conducting properties.[13–19] The EMI shielding effectiveness depends on the intrinsic conductivity, and the dispersion quality of the particle in the composites.[13–15]

In this study, various strategies to tune the localization of MWNTs in a given phase of a bi-phasic blend have been adopted in order to design materials with high electrical conductivity and EMI shielding effectiveness. In order to improve the dispersion quality and to selectively localize MWNTs in the PC phase of the blends, NH_2 terminated MWNTs were adopted. To accomplish this, EDA was grafted on to MWNTs by two different strategies and were compared with respect to commercially available NH_2 terminated MWNTs (hereafter referred to as MWNT-I). In the first approach, EDA was grafted on to MWNTs by diazonium reaction of *para*-substituted benzene ring of MWNT (hereafter referred to as MWNT-II) and in the second approach carboxyl functionalized MWNTs were reacted with thionyl chloride to yield EDA grafted MWNTs (hereafter referred to as MWNT-III). XPS analysis further confirmed the highest surface coverage of EDA on MWNT-III. By this approach we could systematically vary the concentration of NH_2 on the surface of MWNTs. Melt rheological measurements revealed chain scission of PC facilitated by *in situ* reaction between PC and the terminal NH_2 groups of EDA during melt mixing. This further led to smaller PC grafts on the surface of MWNTs and was observed to be dominant in the case of MWNT-III. The observed viscoelastic properties in the blends were correlated with the phase morphologies under quiescent and annealed conditions. Interestingly, MWNT-II showed improved electrical conductivity and EMI shielding in the blends. The observed properties in the blends were correlated with the degree of chain scission in PC.

Experimental

Materials

Polycarbonate (PC), Lexan with MFI of 11 g/10 min was obtained from SABIC. Poly(styrene-*co*-acrylonitrile) (SAN) (M_w of 165 000 g mol^{-1}) was procured from Sigma Aldrich. Different MWNTs like pristine (p-MWNTs, average diameter and length of 9.5 nm and 1.5 μm respectively), NH_2 terminated (MWNT-I, average diameter and length of 9–10 nm and 600–700 nm respectively) and carboxyl functionalized multiwall carbon nanotubes (COOH-MWNTs, average diameter and length of 9.5 nm and 1.5 μm respectively) were procured from Nanocyl SA (Belgium). Analytical grades of sodium nitrate ($NaNO_2$), sulfuric acid (H_2SO_4), thionyl chloride ($SOCl_2$), tetrahydrofuran (THF) and ethylenediamine (EDA) were obtained commercially and were used without further purification.

Blend preparation

Control blends of PC/SAN (50/50, w/w) and with different functionalized MWNTs at a fixed concentration of 1 wt% were prepared, under N_2 atmosphere, by melt blending using Haake minilab II at 260 °C for 20 min and screw speed of 60 rpm. Prior to melt blending, PC and SAN were dried overnight in a vacuum oven at 80 °C. PC was additionally dried for 4 h at 120 °C to remove traces of moisture.

Synthesis of MWNT-II and MWNT-III

EDA was grafted on to MWNTs by a procedure reported earlier.[20] Typically, p-MWNTs (100 mg), EDA (122 mg) and $NaNO_2$ (133 mg) were mixed in a 50 ml round bottomed flask. The mixture was bath sonicated for 20 min. Concentrated H_2SO_4 (87 μl) was added drop wise and heated at 60 °C for 2 h. After completion, the reaction mixture was washed with dimethyl formamide (DMF) and water several times to remove the unreacted EDA. The product was dried in vacuum oven for 24 h at 60 °C to yield EDA-*g*-MWNTs (MWNT-II). MWNT-III was synthesized by acylation of COOH–MWNTs with thionyl chloride. Typically, 200 mg of COOH–MWNTs were dispersed in 20 ml of $SOCl_2$ and was heated at 65 °C for 24 h. The reaction mixture was further stirred in presence of EDA for 24 h at 80 °C. Reaction product was filtered through PTFE membrane (0.22 μm) and washed several times with THF to remove excess EDA. The final product was then dried in vacuum oven for 24 h at 80 °C to yield MWNT-III.

Characterization

Fourier transfer infrared spectroscopy (FTIR) spectra on surface modified MWNTs were recorded using KBr pellet by Perkin Elmer frontier in the range of 650 to 4000 cm^{-1}. Kratos Analytical instrument comprising of Al source was used to record the X-ray Photon Scattering (XPS) on EDA functionalized MWNTs. The Raman spectra for MWNTs were recorded using (LabRAM HR (UV)) spectrophotometer.

Alpha-N Analyzer, Nova Control (Germany) was used to measure the electrical conductivity of the blends at room temperature in the frequency range of 0.1 Hz to 10 MHz. Extruded strands were polished to uniform finish and were sandwiched between the gold electrodes to measure the electrical conductivity.

Localization of MWNTs and morphology of the blends was characterized using scanning electron microscopy (SEM) at 10 kV accelerating voltage. Extruded strands were cryofractured and etched with 30 wt% sodium hydroxide (NaOH) solution for 2 h at 105 °C to remove the PC phase of the blends. This was done to improve the phase contrast of the samples in SEM. Prior to SEM, all the samples were washed with hot water for 15 min and dried in vacuum oven before sputtering with gold. Rheological experiments were performed using a 25 mm diameter parallel plate geometry and 1 mm gap using a Discovery hybrid

rheometer (DHR-3, TA instruments) under N_2 atmosphere. Prior to experiments, strands were dried overnight in a vacuum oven at 80 °C. Isothermal frequency sweeps were carried out in the linear viscoelastic range (determined *apriori*) at 260 °C in the frequency range of 100 rad s^{-1} to 0.1 rad s^{-1}. The evolution of viscoelastic properties under quiescent conditions (0.1 rad s^{-1}, 1% strain) and after applying a steady shear rate of 1 s^{-1} for 10 s was monitored at 260 °C.

Time dependent evolution of AC conductivity in the blends before and after applying a steady shear rate was evaluated by a rheo-electric set up. For this purpose, the rheometer (DHR-3, TA instruments) was coupled to an LCR meter (Agilent E4980A). In a three step experiment, the evolution of AC conductivity as a function of time was evaluated. In the first step, the samples were annealed for 30 min at 260 °C and the evolution of AC electrical conductivity was monitored. In the second step, a steady state shear rate of 1 s^{-1} was applied for 10 s and in 3rd step evolution of AC conductivity with respect to time after the applied shear rate was measured for 30 min. All experiments were performed in linear viscoelastic region and electrical measurements were carried out at constant frequency of 1 kHz.

EMI shielding effectiveness was characterized using Anritsu MS4642A Vector Network Analyzer (VNA) in the X and K_u-band frequencies. The VNA was coupled to a coax set-up (Damaskos M 07T). Two port full SOLT calibration of setup was carried out. The donut shaped specimens were used and the *S* parameters (S_{11}, S_{22}, S_{12} and S_{21}) were recorded in a wide range of frequencies.

Result and discussion

Synthesis and characterization of EDA functionalized MWNTs by different strategies

One pot synthesis of EDA grafted MWNTs (MWNT-II) is carried out in accord with well established diazonium reaction of *para*-substituted benzene ring of CNT with EDA (see Scheme 1a).[20–23] In this case, $NaNO_2$ initiates the semi-stable diazonium ion and subsequently EDA is attached on the surface of MWNTs by radical reaction of diazonium ion with MWNTs.[20,24,25] Ungrafted EDA was removed by washing with DMF and water for several times.

MWNT-III was synthesized by a two-step reaction as shown in Scheme 1b. Grafting of EDA on the MWNT surface was accomplished by acylation with thionyl chloride ($SOCl_2$) at 65 °C for 24 h followed by amidation of MWNT–COCl using EDA at 80 °C. Excess of EDA was removed by washing the reaction product with THF several times. The successful grafting of EDA on the surface of MWNT was further confirmed by FTIR and XPS. As mentioned, one of the motivations behind functionalizing MWNTs with EDA was to facilitate *in situ* reaction between PC and $-NH_2$ functional groups during melt-mixing. This further can result in selective localization of MWNTs in the PC phase. In order to systematically vary the concentration of primary amine on the surface of MWNTs, we also employed commercially available NH_2-MWNTs (MWNT-I). Fig. 1a shows the FTIR spectra of commercially available NH_2 MWNTs (MWNT-I) and EDA grafted MWNTs synthesized *via* two different strategies. The appearance of peak at 1019 cm^{-1} in the FTIR spectra is assigned to the characteristic stretching vibration of C–N, which affirms the presence of amine on the surface of MWNTs. In the case of MWNT-III, the characteristic stretching peak of amide carbonyl (C═O) at 1653 cm^{-1} is also evident. In addition, the appearance of N–H stretching vibration at 3359 cm^{-1} further asserts the presence of primary amine on the surface of MWNTs.[20,26] Further evidence of grafting EDA on to MWNTs was confirmed using XPS. As an example, the XPS of MWNT-II is shown in Fig. 1b. The peak at 398.1 eV, corresponding to N_{1s}, in the XPS spectra confirms the presence of amine group ($-NH_2$).[27] The XPS analysis reveals that the % concentration of N in MWNT-I, MWNT-II and MWNT-III are 0.66, 3.01 and 22 respectively. The significant increase in the % N further confirms the fact that in the case of MWNT-III, the surface coverage of EDA is the highest. This will in turn facilitate selective localization of MWNTs in the PC phase of the blends.

Structural changes in MWNTs on account of functionalization process were assessed using Raman spectroscopy. Fig. 1c shows the Raman spectrum of MWNT-I, MWNT-II and MWNT-III. Two signature peaks are observed in the spectra, one corresponding to the graphitic structure (G-band) at 1584 cm^{-1} and the other related to defect (D-band) at 1337 cm^{-1} is well evident. The intensity ratio, (I_D/I_G) of MWNT-II is 1.44 which is significantly lower than in the case of MWNT-III which is 1.57. It is important to stress that the defect ratio in conventional two step functionalizing route of CNTs is significantly higher than the one pot synthesis approach. The I_D/I_G ratio of the commercially obtained MWNT-I is the lowest.

The successful surface modification of MWNTs *via* EDA has resulted in stable dispersion in polar solvents for several weeks. Fig. 1d shows the representative vials where different MWNTs were dispersed in polar aprotic solvent like DMF. It is evident that NH_2-MWNTs (vial I) settle quickly after the initial sonication process whereas on surface modification with EDA, the dispersions are quite stable (vials II and III). It is envisaged that short EDA chains on the surface of MWNTs will impede the core–core van der Walls' interaction between MWNTs.

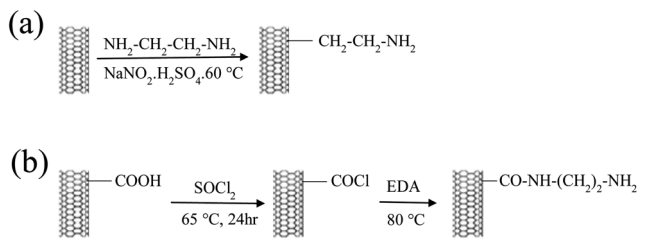

Scheme 1 (a) One pot synthesis of EDA grafting on MWNTs (MWNT-II) and (b) two step strategy to functionalize COOH–MWNTs with EDA (MWNT-III).

Selective localization of MWNTs and phase morphology

We now make an attempt to predict the localization of MWNTs in PC/SAN blends with respect to the thermodynamic criterion. This is accomplished by knowing the surface free energy values

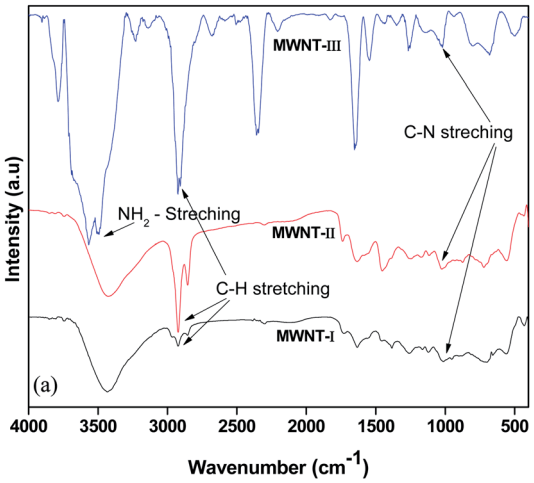

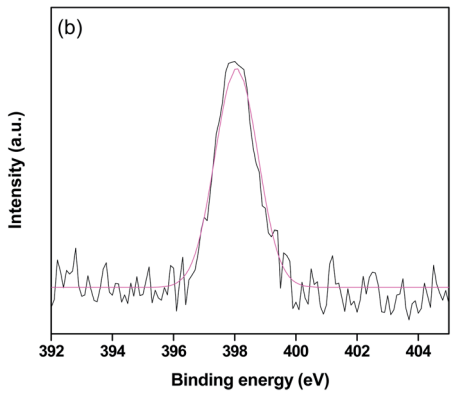

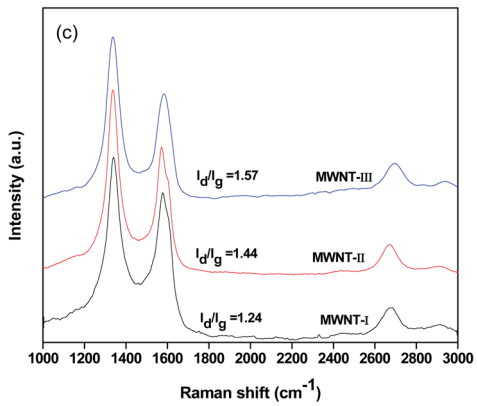

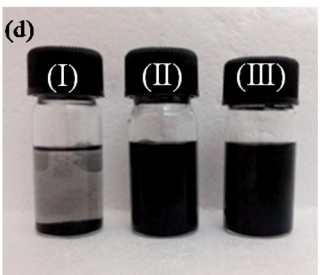

Fig. 1 (a) FT-IR spectra of different MWNTs, (b) XPS for MWNT-II (c) Raman spectra of different MWNTs (d) dispersion of MWNT-I (vial I), MWNT-II (vial II) and MWNT-III (vial III) in DMF.

(at the melt mixing temperature) of the entities and its dependence on temperature. Further, it is assumed that the SFE of MWNTs is weakly dependent on temperature. By estimating the wetting coefficient, as proposed by Sumita *et al.*,[8] given by the following relation one can predict, *apriori*, the localization of particles in a biphasic blends.

$$\omega_{12} = \frac{\gamma_{T2} - \gamma_{T1}}{\gamma_{12}}$$

where, γ_{T1}, γ_{T2} and γ_{12} are the interfacial energies between MWNT/PC, MWNT/SAN, and PC/SAN respectively. If $\omega_{12} > 1$, MWNTs would selectively localize in the SAN phase, for $\omega_{12} < -1$, MWNTs would preferentially localize in the PC phase and for $-1 < \omega_{12} < 1$, MWNTs would localize at the PC/SAN interface. Interfacial tension between the components were calculated by geometric and harmonic mean relations given by,[28]

$$\gamma_{12} = \gamma_1 + \gamma_2 - 4\left(\frac{\gamma_1^d\gamma_2^d}{\gamma_1^d + \gamma_2^d} + \frac{\gamma_1^p\gamma_2^p}{\gamma_1^p + \gamma_2^p}\right)$$

$$\gamma_{12} = \gamma_1 + \gamma_2 - 2\left(\sqrt{\gamma_1^d\gamma_2^d} + \sqrt{\gamma_1^p\gamma_2^p}\right)$$

γ_1, γ_2 are surface free energies (SFE) of PC and SAN respectively. γ_1^d, γ_2^d are disperse and γ_1^p, γ_2^p are the polar components of the surface free energies of PC and SAN respectively. Geometric mean approach is often adopted to calculate the interfacial energies when the SFE values for the components exceed 20 mN m^{-1}.[29] As the MWNTs used in this study are surface modified by EDA, the surface polarity is expected to be higher with respect to unmodified MWNTs. Hence, we assume the SFE for functionalized MWNTs to be 45.3 mN m^{-1}.[30] Table 1 lists the SFE values for PC, SAN and MWNTs at 260 °C. Interfacial energies calculated by geometric mean relationship and the wetting coefficients are summarized in Table 2. Negative wetting coefficients suggest that MWNTs prefer PC phase. It is important to stress at

Table 1 Surface energy and percent polarity values of components at 260 °C. Surface energy value for MWNTs was taken from ref. 30

Materials	Surface energy (mJ m^{-2})	Polarity (%)
PC	30.5	26
SAN	29.5	24
MWNT[30]	45.3	59

Table 2 Thermodynamic parameters calculated using geometric mean equation

	Interfacial energy (mJ m^{-2})		Wetting coefficient
System	GM	System	GM
PC/SAN	0.02	PC/SAN/MWNT	−37.05
PC/MWNT	5.73		
SAN/MWNT	6.47		

this point that the melt viscosity of PC is higher than that of SAN. However, MWNTs are energetically favored towards the PC phase. Furthermore, specific interactions between NH_2 terminal groups in MWNTs and the ester groups in PC further promote the localization of MWNTs in the PC phase.[31]

Fenouillot *et al.*[32] reported that localization of nanoparticles is often governed by rapid diffusion of particles in the lower viscosity phase even if it is thermodynamically unfavorable. In this study, zero shear viscosity of PC and SAN is 1943 Pa s and 930 Pa s respectively, which manifests that MWNTs would prefer to localize in the lower viscous component (here SAN). In order to promote localization of MWNTs in the PC phase, we adopted different strategies like functionalizing MWNTs by EDA. This will in turn result in selective localization of MWNTs in the PC phase of the blend through specific interactions between EDA and PC.[33] A cartoon further illustrates this effect (see Fig. 2).

The phase morphology and the selective localization of MWNTs in the blends are assessed using SEM. In the SEM images shown in Fig. 3, PC phase has been etched out to improve the contrast between the phases. The dispersed PC phase can be seen in a continuous SAN matrix. Interestingly, the blends at this particular composition (and the viscosity ratio) do not yield a co-continuous morphology (see Fig. 3a). However, in presence of different MWNTs (especially MWNT-I and MWNT-II) the phase morphology appears to be refined with respect to the droplet sizes (see Fig. 3b1 and c1). More interestingly, in presence of MWNT-III the blends show a co-continuous microstructure (see Fig. 3d1). This difference in morphology is closely related with the viscosity ratio. We will re-visit this discussion when we discuss melt-rheology.

The high resolution SEM images clearly show the presence of MWNTs in the (etched out) PC phase. As the characteristic length scales of MWNTs are longer than the droplet diameter, few nanotubes are observed in the etched out regions (see Fig. 3b2, c2 and d2). Selective localization of MWNTs in the PC phase is facilitated by the melt-interfacial reaction between amine terminal groups on the surface of MWNTs and the ester groups of PC. It is envisaged that this type of interaction can also lead to chain scission in PC resulting in a decrease in the melt viscosity and will be discussed in more details in the subsequent discussions. Although, the decrease in melt viscosity of PC might facilitate efficient dispersion of MWNTs in the PC phase it might as well result in smaller PC grafts on the surface of MWNTs. The latter however, is contingent upon the degree and extent of reaction. As one of the rationales of this study was to systematically study the effect of concentration of NH_2 terminal groups on the chain scission of PC, we employed different MWNTs with different extent of NH_2 terminal group on their surface.

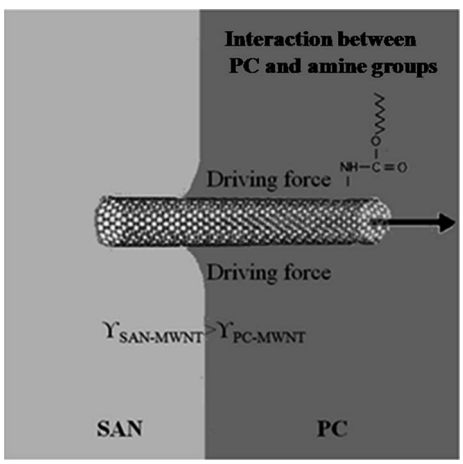

Fig. 2 A cartoon illustrating the driving force behind selective localization of MWNTs in the PC phase.

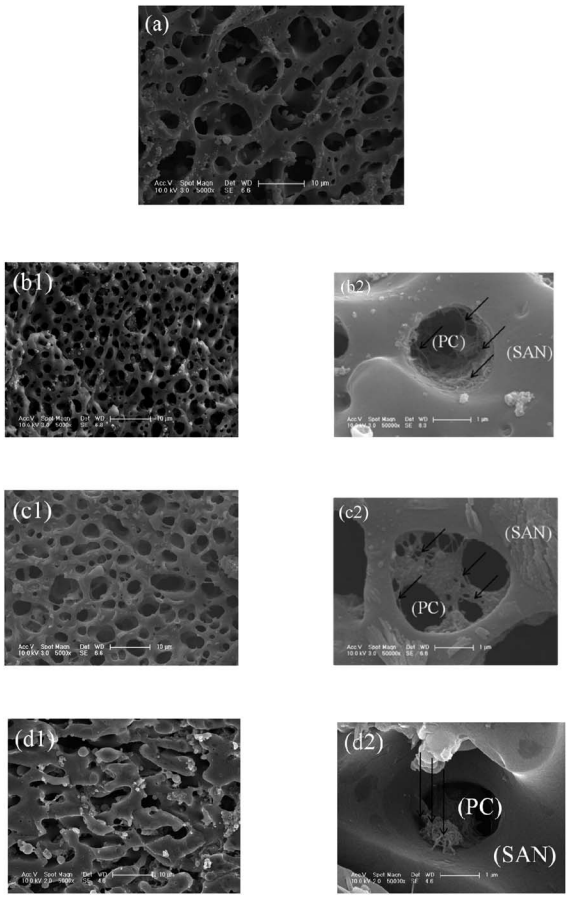

Fig. 3 SEM images of cryofractured extruded strands where PC phase was etched out. (a) Neat blend and blends with MWNT-I (b1 and b2), MWNT-II (c1 and c2) and MWNT-III (d1 and d2).

Melt-rheology: chain scission of PC and efficient dispersion of MWNTs

Fig. 4a shows the variation of complex viscosity as a function of frequency for control blends and with different MWNTs. In the case of neat blends the melt viscosity is almost frequency independent in the measured frequency range however, upon addition of different MWNTs a strong shear thinning effect with a pronounced yield stress at low frequencies is observed. The latter phenomenon is often related with the network build-up of macromolecules and MWNTs in polymeric composites resulting in pseudo-solid like characteristics. This phenomenon is more pronounced in blends with MWNT-I. The increase in melt

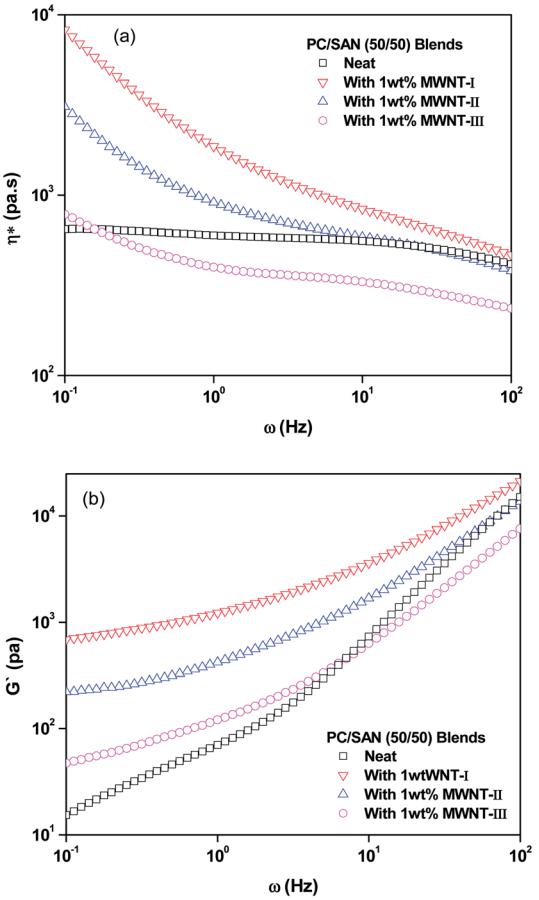

Fig. 4 (a) Complex viscosity as a function of frequency (b) storage modulus as a function of frequency for PC/SAN (50/50) blends with different types of MWNTs.

viscosity is also contingent on the specific interactions between MWNTs and the PC phase as discussed earlier. An important observation draws our attention here. In case of blends with MWNT-III, the melt viscosity especially at higher frequencies is significantly lower than neat blends. This decrease in melt viscosity is often related to either plasticization or a decrease in molecular weight due to chain scission. The DSC scans (not shown here) revealed that the glass transition temperature of PC is nearly unchanged in these blends and hence, the latter phenomenon *i.e.* chain scission looks the more probable cause behind observed decreased in melt viscosity at higher frequencies in our case. This phenomenon was also supported by observation of lower torque values during melt mixing. More interestingly, this observation is also contingent on the concentration of NH_2 terminal groups on the surface of MWNTs with MWNT-III being the highest (as observed from XPS). Such observations were earlier reported and were related with the chain scission of PC.[31] Further confirmation comes from the NMR spectra (not shown here) where the peak at 4.1 ppm corresponding to the –OH terminal groups in PC was observed to be prominent as compared to neat blends suggesting that the population of –OH groups are higher. A cartoon illustrating a possible chain scission mechanism of PC in presence of EDA functionalized MWNTs is displayed in Scheme 2 for a better understanding. From the melt-rheological investigation it is evident that the chain scission in PC is strongly dependent on the critical concentration of NH_2 terminal groups on the surface of MWNTs.

The network formation between polymer chains and MWNTs is also evident in the storage modulus plots. A plateau in the lower frequencies is often observed due to interconnected network resulting in a yield stress. At low frequencies, where sufficient time is available for molecular relaxations, higher modulus is attributed to network formation of particles in the composites.[34] Fig. 4b shows the storage modulus *versus* frequency plots of different compositions studied here. The increase in storage modulus in presence of MWNTs especially at lower frequencies is an indication of the physical network formation of polymer chains and MWNTs. This physical network results in restricted molecular motions of the polymer chains yielding elasticity in the system. It is interesting to note that the storage modulus is highest for MWNT-I followed by MWNT-II and MWNT-III. It is worth recalling that this order is also related to increasing concentration of NH_2 terminal groups on the surface of MWNTs. At higher frequencies, especially for blends with MWNT-III the storage modulus is substantially lower in contrast to neat blends due to chain scission of PC. These blends behave less elastic at higher frequencies as the molecular motion of low molecular weight PC chains is less hindered. The molecular chain scission in PC is limited in MWNT-I and MWNT-II on account of lower content of NH_2 terminal groups on the surface of MWNTs.

Time dependent morphology: effect of MWNTs

Time dependent morphology is industrially relevant especially from post processing operations. In order to understand the effect of time dependent morphology on the overall state of dispersion of MWNTs in the blends, the samples were annealed for 1 h at the processing temperature (260 °C) and the evolution of storage modulus was recorded. Fig. 5 shows the evolution of storage modulus as a function of time for the blends studied here. It is interesting to note that in the case of neat blends, the storage modulus decreases as a function of time indicating coarsening of the phases further, resulting in a reduction of interfacial area.[35] The corresponding phase morphology well supports this observation. More interestingly, in the case of blends with different MWNTs a distinct change in the storage modulus is observed in striking contrast to the neat blends. The storage modulus increases as a function of time in the blends with MWNTs. Annealed morphologies of the blends in presence of different MWNTs although coarsened represent a continuous PC phase (Fig. 5). It is well envisaged that interpenetrated structures like co-continuous morphologies and pseudo solid like network of MWNTs gives rise to elasticity. The contribution to storage modulus from these two effects is from the same physical origin leading to an increase in storage modulus in the blends. The extent of increase in storage modulus is again observed to be contingent on the concentration of NH_2 functional groups present on the surface of MWNTs. The network formation of MWNTs in the melt state can be explained by

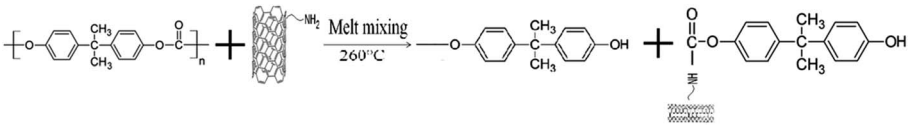

Scheme 2 Possible chain scission mechanism of PC in presence of NH_2 terminated MWNTs.

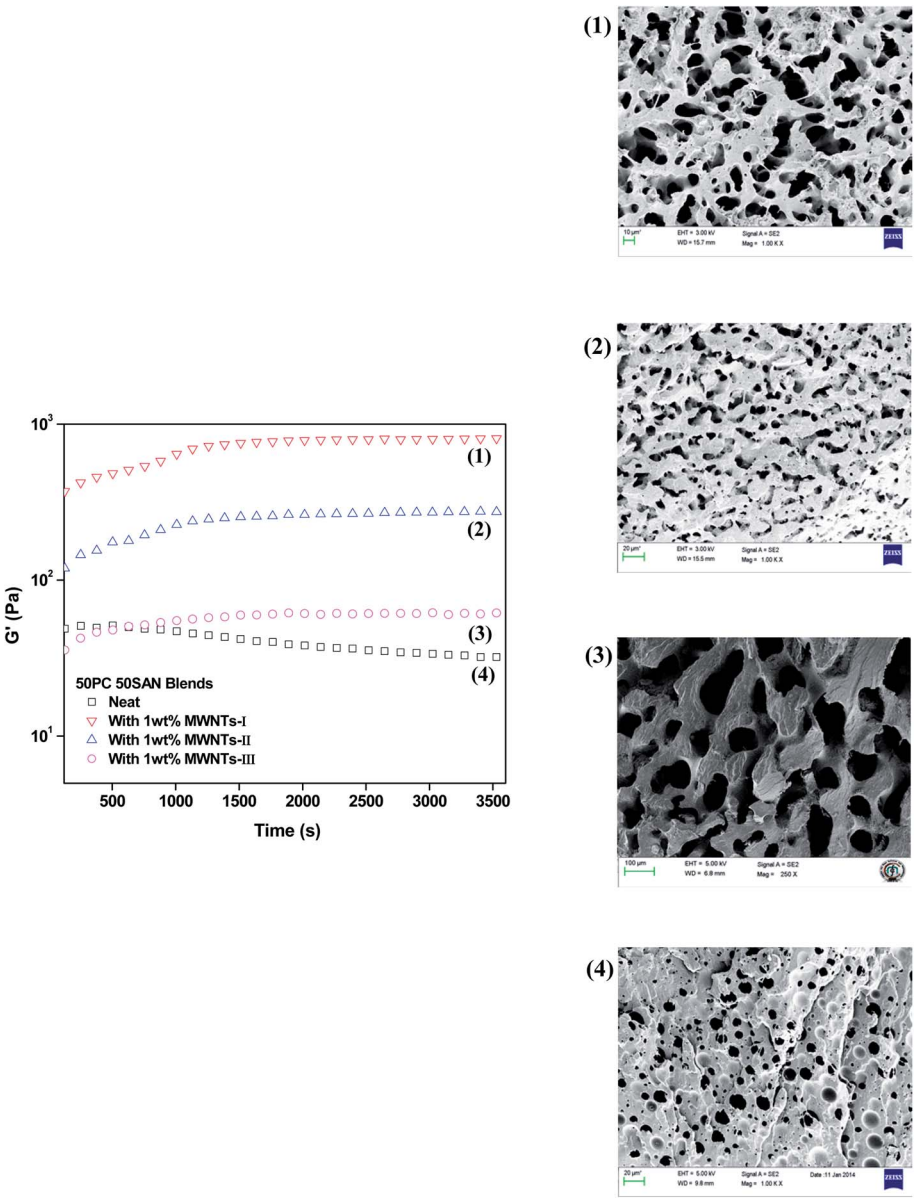

Fig. 5 Storage modulus as a function of annealing time. The corresponding morphologies are shown as inset.

diffusion of MWNTs in the macromolecules. The melt viscosity of PC in case of blends with MWNT-III is low. However, more number of PC grafts attached to the surface of MWNTs hinders the mobility of MWNTs. This possibly could explain the observed lower storage modulus after isothermal annealing. The dispersion state of different MWNTs and the subsequent network formation is studied here in more details by electro-rheology set up. As mentioned earlier, an LCR meter is coupled to a rheometer to record the electrical conductivity of the blends both under quiescent and steady shear conditions.

Time dependent morphology: assessing through electro-rheological measurements

In this section, both the electrical conductivity at room temperature and in the melt state is discussed. While the room

temperature conductivity is relevant to many applications, the electrical conductivity in the melt state allows systematic understanding of the network buildup of MWNTs. Fig. 6 shows the frequency dependent AC electrical conductivity of blends in presence of different types of MWNTs. In order to realize the double percolation effect on the overall bulk electrical conductivity of the blends, composites of PC with 1 wt% MWNT-I is also prepared under the same melt mixing conditions. Interestingly, this particular composite exhibit insulating characteristics. On the other hand, blends with MWNT-I and MWNT-II reveal significantly high electrical conductivity in striking contrast to neat PC/SAN blends or PC/MWNT-I composites. Percolation threshold for rod-like conducting fillers can be predicated by percolation theory ($p_c = D/2L$; D and L corresponds to diameter and length of the filler), which clearly indicate that percolation threshold (p_c) decreases with increase in aspect ratio of conducting filler.[33]

The frequency independent plateau at lower frequencies is an indication of network formation of MWNTs in a given phase of the blends. Interestingly, blends with MWNT-II shows a dramatic seven orders of increase in AC electrical conductivity in striking contrast to neat blends. Moreover, the frequency independent plateau extends to 1 MHz. This observation is a manifestation of selective localization of MWNTs in the PC phase of the blends. In an earlier work by Potschke *et al.*[36] the DC conductivity of PC, SAN and PC/SAN blends were compared. Composites of PC and SAN showed higher percolation threshold, which is 1.5 and 2 wt% respectively, as compared to PC/SAN blends which rather showed significantly lower percolation threshold *ca.* 1.2 wt% of MWNTs. One important criterion is worth analyzing here. Although we have adopted three different MWNTs in order to systematically vary the concentration of NH_2 terminal groups on the surface of MWNTs, the characteristic length scales of these nanotubes are different. The length scales of MWNT-II and MWNT-III are although similar however, the length scale of MWNT-I is smaller by a factor of two. These variations in the length scales are directly related with the functionalization process adopted and consequently on the integrity of the tubes in electron tunneling. More defects are induced in the conventional functionalization process like treating the MWNTs with harsh acids. In order to avoid such a process, we employed a one-pot synthesis of EDA functionalized MWNTs which resulted in fewer defects in striking contrast to conventional processes of functionalizing MWNTs. This was also supported by Raman spectroscopy. Hence, the observed higher electrical conductivity in the case of MWNT-II is related with higher aspect ratio of the MWNTs. Moreover, by facilitating selective localization of MWNTs in a given phase higher electrical conductivity is often achieved at a relatively lower fraction of MWNTs. While, the electrical conductivity of the blends with MWNT-II can be explained based on its length but the observed lower conductivity in the blends in presence of MWNT-III with respect to MWNT-I needs a closer inspection. As mentioned, MWNT-I is shorter by a factor of 2 with respect to MWNT-III although, the conductivity is higher in MWNT-I. We expect higher number of PC grafts on the surface of MWNT-III resulting in an insulating coating of PC. Moreover, on account of chain scission of PC, the viscosity of PC has decreased. This might result in good dispersion of MWNTs in PC phase thereby reducing the nanotube–nanotube contact. The latter is a pre-requisite for high electrical conductivity.

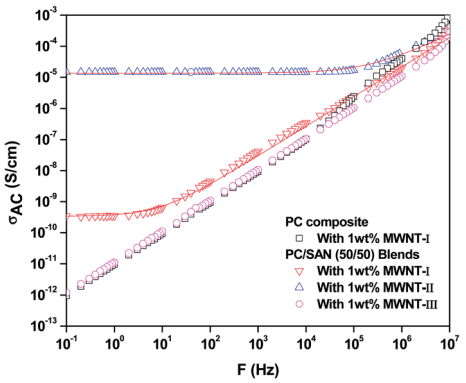

Fig. 6 AC conductivity as a function of frequency for PC/SAN (50/50) blends with different MWNTs.

The power law behavior[37,38] of frequency dependent AC conductivity at room temperature was further analyzed using the following equation.

$$\sigma'(\omega) = \sigma(0) + \sigma_{ac}(\omega) = \sigma_{dc} + A\omega^s$$

where, σ_{dc} is DC conductivity, A is temperature dependent constant, ω is angular frequency and s is both temperature and frequency dependent exponent with value ranging from 0 to 1. The σ_{dc} values were estimated by fitting the power law. Various parameters like DC conductivity (σ_{dc}), crossover frequency (f_c) and exponent 's' were estimated using the power law discussed above. The value of exponent 's' in the case of MWNT-III is 0.75 indicating 75% resistance and 25% capacitance equivalent network.[39] Similarly, for a-MWNTs resistance network and capacitance network is 95% and 5% respectively.

As briefly mentioned before that the random percolation of MWNTs greatly depends on the medium viscosity and the characteristic length scales. In order to gain more insight in the random percolation of different MWNTs employed here, we monitored the evolution of electrical conductivity in the melt state under isothermal annealing and also under shear. The latter is employed to locally disturb the network of MWNTs and assess the subsequent network build-up. Fig. 7 shows the evolution of AC electrical conductivity as a function of time under isothermal annealing (at 260 °C). It is envisaged that at higher temperature random percolation of MWNTs is facilitated in the melt. The blends with different MWNTs showed higher AC electrical conductivity in striking contrast to room temperature conductivities. This is related with random network formation of MWNTs or MWNT agglomerates in the melt state by diffusion. Initially, the AC conductivity was monitored under quiescent conditions *i.e.* isothermal annealing for 30 min. Later on the AC conductivity was monitored after applying a steady state shear rate of 1 s^{-1} for 10 s. The AC

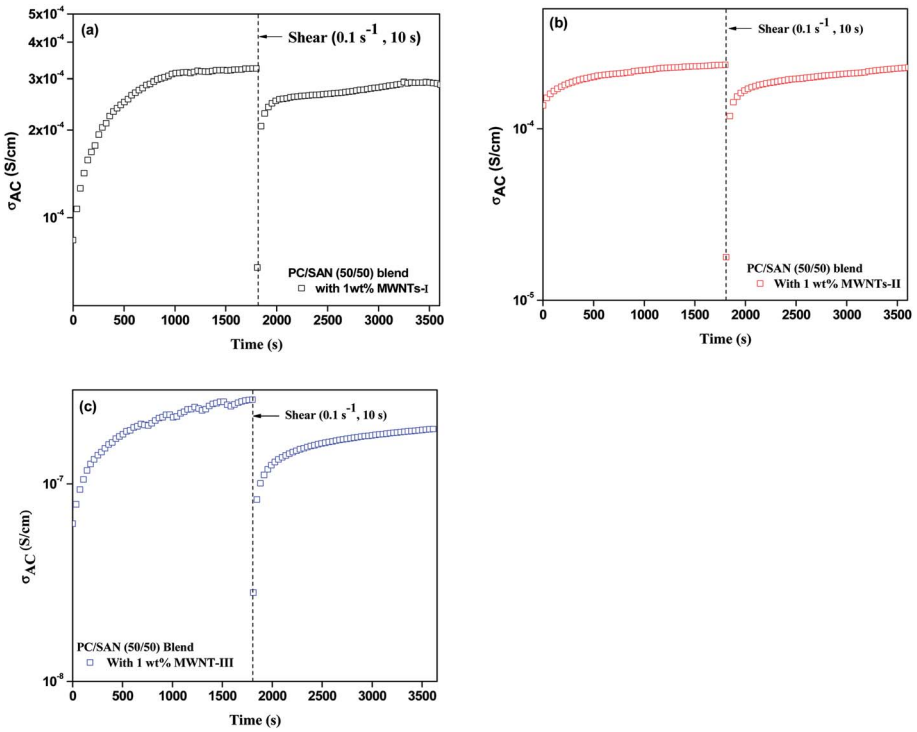

Fig. 7 AC conductivity as a function of time under quiescent and after cessation of shear for PC/SAN (50/50) blends with (a) MWNT-I (b) MWNT-II and (c) MWNT-III.

conductivity is observed to increase as a function of time due to random network formation of MWNTs in the PC phase during isothermal annealing. After applying a steady shear, the AC conductivity decreases marginally which can be explained by shear induced destruction of MWNT network. It is worth stressing at this point that shear can also alter the phase morphology in the blends. For instance, higher shear rates can reduce the surface tension more significantly resulting in string-like domains. After the cessation of steady shear, the surface tension will again start to increase resulting in an interfacial contribution to storage modulus. The morphology attained after the cessation of shear is not at equilibrium and the morphology will coarsen as a function of time which to some extent is arrested in the case of blends with MWNTs. In an earlier work by Potschke *et al.*, the PC composites with MWNTs showed a greater decrease in electrical conductivity[34,40] at similar shear rates used in this work. However, in the case of blends, the conductivity only reduced marginally. One possible reason could be that in the case of blends, higher degree of shear is needed to break down the network of MWNTs or MWNT agglomerates as they are packed quite closely in a given phase. The recovery of AC conductivity after the cessation of shear was observed due to reformation of MWNTs or MWNT agglomerate network. In case of MWNT-I, the conductivity increases with time due to random network formation in the melt state and saturates after 1000 s. Blends with MWNT-II, where in the network of MWNT has been already formed showed only a marginal increase in the conductivity with annealing time, whereas, the time required to form network of MWNTs is quite high in the case of MWNT-III. This could possibly be due to small diffusion rate of MWNT-III in the PC phase. The viscosity of the PC phase is significantly lower in presence of MWNT-III and hence, the diffusion rate is expected to be higher. However, smaller PC grafts on the surface of MWNTs impede the network formation and result in longer time scales to form random percolation network. A cartoon illustrating the effect of concentration of NH_2 terminal groups on the chain scission and diffusion rate of MWNTs in the PC phase (Fig. 8).

EMI shielding: effect of different MWNTs

By tuning the localization of MWNTs in the PC phase, materials with high electrical conductivity can be designed. Such materials can further be explored as EMI (electromagnetic interference) shielding materials. The EMI shield effectiveness (EMI SE) is the ratio of electromagnetic radiation transmitted through the shielding material to incident electromagnetic radiation. This can be estimate from magnetic (H), electric (E) and electromagnetic power (P) as given below.[41,42]

$$SE_T(dB) = -20 \log \frac{E_T}{E_I} = -20 \log \frac{H_T}{H_I} = -10 \log \frac{P_T}{P_I}$$

In the vector network analyzer (VNA), EMI SE is represented in terms of scattering parameters (S_{11}, S_{22}, S_{12} and S_{21}). The total EMI SE can be evaluated from the S parameters using the below relation.

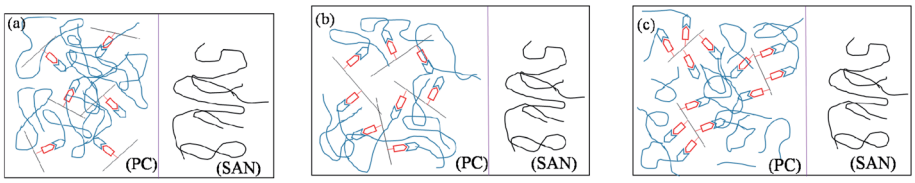

Fig. 8 A cartoon illustrating the effect of concentration of NH_2 terminal groups on the chain scission of PC. (a) MWNT-I (b) MWNT-II and (c) MWNT-III.

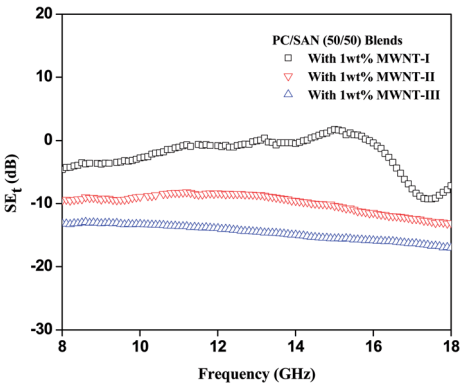

Fig. 9 Plot of frequency *versus* total shielding effectiveness for filled PC/SAN (50/50) blends with different types of MWNTs.

$$SE_T(dB) = 10 \log \frac{1}{|S_{12}|^2} = 10 \log \frac{1}{|S_{21}|^2}$$

Fig. 9 shows the SE in the X (8–12 GHz) and K_u-band (12–18 GHz) which are of commercial importance. Interestingly, blends with MWNT-I and MWNT-II exhibit a SE of 8.4 dB and 14 dB in both the frequency regimes. Whereas, MWNT-III shows very low SE which is 3 dB. Grafting of EDA on MWNTs by one pot synthesis method (*i.e.* MWNT-II) resulted in SE which is of commercial and industrial relevance. PC/SAN blends with MWNT-II showed significantly high SE value at very low concentration of MWNTs. A recent review highlights the SE of polymer based composites using carbonaceous filler and it is well understood that the blends with MWNT-II exhibited significantly higher SE at very low fraction of MWNTs.[43] By increasing the fraction of MWNT-II in the blends, SE can be enhanced further. As the loading of the nanoparticles increases, processing becomes difficult and hence, achieving desired properties at lower fraction of nanoparticles are in great demand. This study can provide new avenues in developing nanocomposites with enhanced EMI SE at lower fractions of conducting particles.

Conclusions

Selective localization and dispersion of as received NH_2 terminated multiwall carbon nanotubes (MWNT-I) and covalently functionalized with EDA using different strategies (MWNT-II and MWNT-III) was assessed here in PC/SAN blends with respect to morphology, rheology and electrical conductivity. The *in situ* reaction of amino group on the surface of MWNTs with the carboxyl linkage of PC during melt blending drives MWNTs in the PC phase. The viscoelastic properties were monitored during isothermal annealing. Higher content of NH_2 terminal groups in MWNT-III led to chain scission of PC. These results further corroborated with the rheo-electrical experiments, both under quiescent and after cessation of shear, where the effect of amine concentration on the diffusion rate of MWNTs and the subsequent network build-up could be effectively mapped. Further, MWNT-II showed enhanced EMI SE in the X and K_u-band frequencies which are of commercial importance. This study can open new pathways to design composites with enhanced electrical conductivity and EMI SE at lower fractions of MWNTs.

Acknowledgements

The authors gratefully acknowledge the Department of Science and Technology (DST), India for the financial support. The authors would also like to acknowledge Prof. Giridhar Madras for the FTIR facility, Center for Nano Science and Engineering (CeNSE), IISc for the characterization facility and Mr. Prasanna Kumar for his assistance in FTIR.

References

1 J. C. Huang, *Adv. Polym. Technol.*, 2002, **21**, 299–313.
2 J.-H. Choi, J. Jegal and W.-N. Kim, *J. Membr. Sci.*, 2006, **284**, 406–415.
3 D. M. Bigg, *Polym. Eng. Sci.*, 1979, **19**, 1188–1192.
4 M. Sharma, K. Sharma and S. Bose, *J. Phys. Chem. B*, 2013, **117**, 8589–8602.
5 C. Zhang, X. S. Yi, H. Yui, S. Asai and M. Sumita, *J. Appl. Polym. Sci.*, 1998, **69**, 1813–1819.
6 G. Wu, S. Asai, M. Sumita and H. Yui, *Macromolecules*, 2002, **35**, 945–951.
7 F. Gubbels, S. Blacher, E. Vanlathem, R. Jérôme, R. Deltour, F. Brouers and P. Teyssie, *Macromolecules*, 1995, **28**, 1559–1566.
8 M. Sumita, K. Sakata, S. Asai, K. Miyasaka and H. Nakagawa, *Poly. Bull.*, 1991, **25**, 265–271.
9 M. Wu and L. Shaw, *J. Appl. Polym. Sci.*, 2006, **99**, 477–488.
10 O. Meincke, D. Kaempfer, H. Weickmann, C. Friedrich, M. Vathauer and H. Warth, *Polymer*, 2004, **45**, 739–748.
11 M. Terrones, *Annu. Rev. Mater. Res.*, 2003, **33**, 419–501.

12 S. Bose, R. A. Khare and P. Moldenaers, *Polymer*, 2010, **51**, 975–993.
13 D. D. L. Chung, *Carbon*, 2001, **39**, 279–285.
14 M. B. Bryning, M. F. Islam, J. M. Kikkawa and A. G. Yodh, *Adv. Mater.*, 2005, **17**, 1186–1191.
15 J. Joo and C. Y. Lee, *J. Appl. Phys.*, 2000, **88**, 513–518.
16 X. Luo and D. D. L. Chung, *Composites, Part B*, 1999, **30**, 227–231.
17 J. Joo and A. J. Epstein, *Appl. Phys. Lett.*, 1994, **65**, 2278–2280.
18 C. Xiang, Y. Pan, X. Liu, X. Sun, X. Shi and J. Guo, *Appl. Phys. Lett*, 2005, **87**, 123103.
19 Y. Yang, M. C. Gupta, K. L. Dudley and R. W. Lawrence, *Adv. Mater.*, 2005, **17**, 1999–2003.
20 W. Chidawanyika and T. Nyokong, *Carbon*, 2010, **48**, 2831–2838.
21 J. L. Bahr, J. Yang, D. V. Kosynkin, M. J. Bronikowski, R. E. Smalley and J. M. Tour, *J. Am. Chem. Soc.*, 2001, **123**, 6536–6542.
22 C. A. Dyke and J. M. Tour, *J. Phys. Chem. A*, 2004, **108**, 11151–11159.
23 B. K. Price and J. M. Tour, *J. Am. Chem. Soc.*, 2006, **128**, 12899–12904.
24 A. Amiri, M. Maghrebi, M. Baniadam and S. Zeinali Heris, *Appl. Surf. Sci.*, 2011, **257**, 10261–10266.
25 M. D. Ellison and P. J. Gasda, *J. Phys. Chem. C*, 2008, **112**, 738–740.
26 H. Peng, L. B. Alemany, J. L. Margrave and V. N. Khabashesku, *J. Am. Chem. Soc.*, 2003, **125**, 15174–15182.
27 V. Penmatsa, H. Kawarada and C. Wang, *J. Micromech. Microeng.*, 2012, **22**, 045024.
28 G. C. Nayak, S. Sahoo, R. Rajasekar and C. K. Das, *Composites, Part A*, 2012, **43**, 1242–1251.
29 P. Pötschke, S. Pegel, M. Claes and D. Bonduel, *Macromol. Rapid Commun.*, 2008, **29**, 244–251.
30 S. Nuriel, L. Liu, A. H. Barber and H. D. Wagner, *Chem. Phys. Lett.*, 2005, **404**, 263–266.
31 J. R. Caldwell and W. J. Jackson, *J. Polym. Sci., Part C: Polym. Symp.*, 1968, **24**, 15–23.
32 F. Fenouillot, P. Cassagnau and J.-C. Majeste, *Polymer*, 2009, **50**, 1333–1350.
33 S. Bose, A. R. Bhattacharyya, A. P. Bondre, A. R. Kulkarni and P. Pötschke, *J. Polym. Sci., Part B: Polym. Phys.*, 2008, **46**, 1619–1631.
34 I. Alig, T. Skipa, D. Lellinger and P. Pötschke, *Polymer*, 2008, **49**, 3524–3532.
35 H. K. Jeon and J. K. Kim, *Polymer*, 1998, **39**, 6227–6234.
36 A. Göldel, G. Kasaliwal and P. Pötschke, *Macromol. Rapid Commun.*, 2009, **30**, 423–429.
37 A. K. Jonscher, *Nature*, 1977, **267**, 673–679.
38 E. Logakis, C. Pandis, V. Peoglos, P. Pissis, J. Pionteck, P. Pötschke, M. Mičušík and M. Omastova, *Polymer*, 2009, **50**, 5103–5111.
39 P. K. S. Mural, G. Madras and S. Bose, *RSC Adv.*, 2014, **4**, 4943–4954.
40 I. Alig, P. Pötschke, D. Lellinger, T. Skipa, S. Pegel, G. R. Kasaliwal and T. Villmow, *Polymer*, 2012, **53**, 4–28.
41 S.-S. Tzeng and F.-Y. Chang, *J. Mater. Sci. Eng. A*, 2001, **302**, 258–267.
42 N. F. Colaneri and L. W. Schacklette, *IEEE Trans. Instrum. Meas.*, 1992, **41**, 291–297.
43 D. D. L. Chung, *Carbon*, 2012, **50**, 3342–3353.

